

Theoretical Inspecting of ^{211}At Radionuclide via Coupled-Channel Model for Fusion Reaction of Stable Nuclei

Z. M. Cinan^{1*}, T. Baskan¹, B. Erol², A. H. Yilmaz¹

¹Department of Physics, Faculty of Science, Karadeniz Technical University, Milli Egemenlik Avenue No.39, Trabzon 61080, Turkey

²Department of Physics, Faculty of Arts and Science, Recep Tayyip Erdoğan University, Zihni Derin Campus, Rize 53100, Turkey

ARTICLE INFO

Article history:

Received 9 January 2021

Received in revised form 5 June 2021

Accepted 7 June 2021

Keywords:

Astatine-211
Coupled channel model
Fusion barrier distributions
Fusion cross sections
Heavy-Ion fusion reaction
Radionuclide

ABSTRACT

This work has been carried out to obtain and inspect of ^{211}At radionuclide through fusion reaction. Cross-sections for fusion reaction have been calculated with different interaction combinations and excitations for $^{19}\text{F} + ^{192}\text{Os}$ and $^{18}\text{O} + ^{193}\text{Ir}$ reactions. All calculations have been performed on NRV Knowledge Base, CCFULL code, and Wong's Formula. Firstly, we assigned reaction parameter values taking into account the compatibility with the experimental data $^{19}\text{F} + ^{192}\text{Os}$ reaction. Afterward, to enrich studies on ^{211}At radionuclide, we proposed $^{18}\text{O} + ^{193}\text{Ir}$ reaction which did not have experimental data in the literature with the method and parameter values we determined. We examined the effects of phonon excitations in projectile and target nuclei on fusion cross sections and barrier distributions. With our research, we showed that the coupled channel model and the calculation codes used to explain the fusion cross-section data and barrier distributions well. This research sheds light on the importance of analyzing important medical radionuclides such as ^{211}At by heavy-ion fusion reactions and encourages new researches.

© 2021 Atom Indonesia. All rights reserved

INTRODUCTION

Fusion mechanisms of heavy-ion interactions have attracted big attention experimentally and theoretically as they reveal the interaction between the nuclear structure and reaction mechanisms [1-4]. Fusion processes at energies near the Coulomb barrier can be considered as a multidimensional barrier penetration problem [5-8]. The multidimensional barrier penetration part can be explained by disentangling the coupled channel (CC) model equations [9-13]. Nevertheless, on account of complex reaction mechanisms, it is obligatory to reckon with a great number of channels that are difficult to perform in the calculation model. In addition, data statistics of the reacting particles are required as input. Whence, coupled channel calculations can happen to challenge in multiple situations.

Different models have been recommended for the coefficients of the barrier distributions concerning the constant and dynamic deformations of the two interacting nuclei, according to the interaction potential between the projectile and the target [13,14]. For the vibrational and rotational coupling effect, the parameters of the models used respectively are given. For spherical reaction systems (vibrational coupling effect), the amplitude of the barrier distribution ascends with the charge product of the reaction system, while for the deformed reaction systems (rotational coupling effect), besides the charge product of the reaction system, the amplitude of the barrier distributions is also related to the static deformation coefficients of the projectile and the target [13-16]. In general, the CC model for the parameters of the barrier distribution works quite well in defining cross-sections and can provide useful information about cross-section estimates [16-18].

*Corresponding author.

E-mail address: m_cinan@ktu.edu.tr

DOI: <https://doi.org/10.17146/aij.2021.1115>

This research deal with the calculation of cross-sections and barrier distributions via coupled channels method for ^{211}At radionuclide, which is one of the most important medical radionuclides. Our research intends to analyze the influence of different interaction combinations and excitations on fusion reactions and investigate the phonon excitations' influence on the cross-sections and barrier distributions. Furthermore, this research sheds light on the importance of analyzing important medical radionuclides such as ^{211}At by heavy-ion fusion reactions.

All calculations were carried out with the use of the web knowledge base NRV [17-21], CCFULL code [14,22], and Wong's Formula [23,24]. The calculation model is briefly summarized in Coupled Channel Model Theory section. The Results and Discussions section involves the outcomes of our calculations, also embracing a collation with experimental data [25]. In the last section, we outlined our outcomes and introduced our consequences.

COUPLED CHANNEL MODEL THEORY

In this section, we briefly summarized coupled channel (CC) model we use in our calculations for heavy-ion fusion reaction systems.

Barrier distribution function, $D(B)$, at the classical limits by using Eq. (1) [14]:

$$D(B) = \frac{1}{\pi R_B^2} d^2 (E\sigma_{fus})/dE^2 \Big|_{E=B} \quad (1)$$

here R_B is the barrier radius, σ_{fus} is fusion cross sections and E is the incident energy in the center of mass frame.

Barrier distribution function is linked to the improved penetration dynamics of the barrier in vigorous channel couplings. Barrier penetration probability $T_l(B;E)$ according to the Hill-Wheeler formula is a function by using Eq. (2) and (3) [26]:

$$x = B + \frac{\hbar^2}{2\mu R_B^2} l(l+1) - E \quad (2)$$

$$T_l(B;E) = f(x) \quad (3)$$

here l indicates the angular momentum between the interacting nuclei.

Reaction cross sections can be written:

$$\sigma_{fus}(E) = \frac{\pi\hbar^2}{2\mu E} \sum_{l=0}^{\infty} (2l+1) T_l(E) \quad (4)$$

If we write the barrier distribution function by using Eq. (4) [27]:

$$\begin{aligned} \frac{d(E\sigma_{fus})}{dE} &= \frac{\pi\hbar^2}{2\mu} \sum_{l=0}^{\infty} (2l+1) \frac{dT_l(B;E)}{dE} \\ &= -\pi R_B^2 \sum_{l=0}^{\infty} (2l+1) \frac{dT_l(B;E)}{dl} \end{aligned} \quad (5)$$

$$\begin{aligned} D(E) = \delta(E-B) &= d^2 (E\sigma_{fus})/dE^2 \\ &= \frac{dT_l(B;E)}{dl} \end{aligned} \quad (6)$$

where μ is the reduced mass, l is the relative angular momentum between the colliding nuclei, $T(E) = 1$ for $E > B$ and $T(E) = 0$ for $E < B$.

Since the potential energy of the reaction system is multidimensional, the incoming flux crosses the Coulomb barrier at variable B height worths (assorted deformations or orientation worths). The potential barrier distribution is directly related to relative motion and the coupling of the interior ranks of freeness for projectile and target nucleus, for example, low excitation rotational state and vibration state with relative motion will produce a strong coupling. Rotation of the nucleus is related to static deformations and the vibration is related to changing the shape of the nucleus. After the projectile and the target nuclei reach a certain distance, the surface of the projectile and target nuclei distorted due to the pull of the nucleus force and the push of the Coulomb force. In this case, the nucleus undergoes deformation [16].

The fusion cross-section computed therein the limits of coupled channel (CC) model is defined by Eq. (4) [18]. Compound nucleus (CN) cross-section calculation in the interactions of the heavy nucleus:

$$\sigma_{fus}^{CN}(E) = \frac{\pi\hbar^2}{2\mu E} \sum_{l=0}^{\infty} (2l+1) T_l(E) P_{CN}(E, l) \quad (7)$$

here $P_{CN}(E, l)$ is the penetration probability for compound nucleus (CN).

Wong's formula for cross sections [23,24]:

$$\sigma(E) = \frac{\hbar\omega}{2E} R_B^2 \ln \left[1 + \exp \left(\frac{2\pi}{\hbar\omega} (E - V_B) \right) \right] \quad (8)$$

In this formula, it can be seen that the cross-section is calculated with the help of three parameters: the curvature $\hbar\omega$, the barrier radius R_B , and the barrier height V_B .

Other than Eq. (8), above and below the Coulomb barrier:

$$\sigma(E) = \pi R_B^2 \left(1 - \frac{V_B}{E} \right) \text{ for } E > V_B \quad (9)$$

$$\sigma(E) \approx R_B^2 \frac{\hbar\omega}{2E} \exp \left(\frac{\hbar\omega}{2E} (E - V_B) \right) \text{ for } E < V_B \quad (10)$$

For the Wong barrier distributions, the following equation is used:

$$\frac{d^2 E \sigma_{fus}}{dE^2} = \pi R_B^2 \frac{2\pi}{\hbar\omega} \frac{e^x}{(1+e^x)^2}; x = \frac{2\pi}{\hbar\omega} (E - V_B) \quad (11)$$

RESULTS AND DISCUSSION

In this section, we submit our calculation results via coupled channels model for ^{211}At radionuclide.

All calculations were carried out with the use of the web knowledge base NRV [17-21], CCFULL code [14,22], and Wong's Formula [23,24] of $^{19}\text{F} + ^{192}\text{Os}$ and $^{18}\text{O} + ^{193}\text{Ir}$ reaction systems. We chose the $^{19}\text{F} + ^{192}\text{Os}$ reaction to determine the theoretical background from the experimental data [25] and then based on the information obtained here we proposed the $^{18}\text{O} + ^{193}\text{Ir}$ reaction which experimental data are not present. We have analyzed respectively the $^{19}\text{F} + ^{192}\text{Os}$ and $^{18}\text{O} + ^{193}\text{Ir}$ reactions cross-sections and barrier distributions at 0.5 MeV steps in the energy range of 70-100 MeV and 60-85 MeV (with nuclear parameter combinations of the projectile and target nuclei with CC model). The parameters of the nuclear potential were established for each reaction and listed in Table 1.

Table 1. Woods-Saxon potential, height, position parameters, and Coulomb barrier of reactions for CC Model.

| System | $V_0(\text{MeV})$ | $r_0(\text{fm})$ | $a_0(\text{fm})$ | $V_C(\text{MeV})$ |
|-----------------------------------|-------------------|------------------|------------------|-------------------|
| $^{19}\text{F} + ^{192}\text{Os}$ | 66.290 | 1.210 | 0.652 | 80.206 |
| $^{18}\text{O} + ^{193}\text{Ir}$ | 63.931 | 1.179 | 0.661 | 72.138 |

The results respectively represent phonons (n=1, 2, 3, 5 and 10) associated with quadrupole (2^+) and octupole (3^-) vibrations combinations of the surface of ^{192}Os target nucleus via ($\lambda = 2^+, \hbar\omega_{2^+} = 0.2058 \text{ MeV}, \langle\beta_{2^+}^0\rangle = 0.1639$) and ($\lambda = 3^-, \hbar\omega_{3^-} = 1.341 \text{ MeV}, \langle\beta_{3^-}^0\rangle = 0.060$) parameters [28-31]. Furthermore, we took the integration parameters as $R_{max} = 25 \text{ fm}$ and integration step $h = 0.05 \text{ fm}$ in our calculations [16,21,32].

For $^{19}\text{F} + ^{192}\text{Os}$ reaction, in executing the coupled channels calculations, we considered the quadrupole (2^+) and octupole (3^-) states and phonon excitations of target nuclei while projectile nuclei were inert. The results of coupled channel model calculations (fusion cross-sections and barrier distributions) were compared and

demonstrated with experimental data in Figs. 1(a,b) and Figs. 2(a,b).

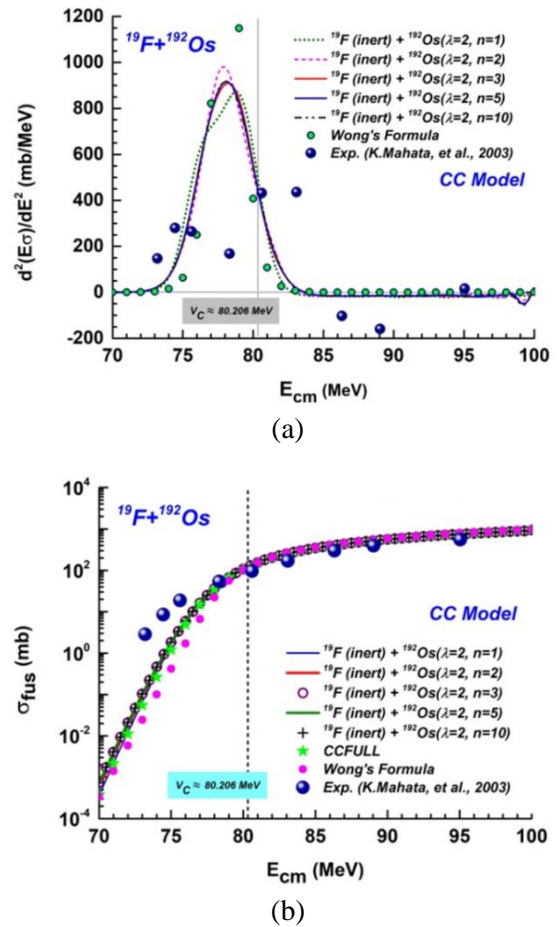


Fig. 1. Graphs of (a) the cross-sections and (b) barrier distributions for $^{19}\text{F} + ^{192}\text{Os}$ the fusion reaction within the coupled channel (CC) model the interactions of the inert projectile and quadrupole (2^+) state of target nuclei.

The blue solid line, red solid line, purple ring, olive green solid line, and black plus line curves represent respectively the phonon excitations (n=1, 2, 3, 5, and 10) of cross-sections were achieved over the interactions of the inert projectile and quadrupole (2^+) state of target nuclei in Fig. 1(a) [17-21]. Neon green stars and magenta circles represent CCFULL and Wong's Formula calculations [14,22-24]. Royal blue balls indicate experimental data for this reaction [25].

The three experimental data (for 73.19, 74.45, and 75.62 MeV) are slightly different from our theoretical calculations in Fig. 1(a). When we approached the barrier region, harmony was observed between other theoretical and experimental values. Theoretical cross-section values change as 53.75, 49.96, 50, 50.41 and 50.47 mb for phonon (from 1 to 10 phonons) excitations at 78.5 MeV while experimental cross-section value is measured as 53.85 mb at 78.33 MeV [25]. It is observed that

coupled channel and phonon excitation effects increased the computed fusion cross-section at energies around the Coulomb barrier.

The olive green short dotted line, magenta short dashed line, red solid line, blue solid line, and black dash-dot dotted line curves represent respectively the phonon excitations ($n=1, 2, 3, 5,$ and 10) of barrier distributions were achieved over the interactions of the inert projectile and quadrupole (2^+) state of target nuclei in Fig. 1(b) [17-21]. Royal blue circles filled with neon green represent Wong's Formula calculations [23,24]. Navy blue balls indicate experimental data for this reaction [25].

Theoretical barrier distribution values change as 441.7, 304.3, 336.8, 336.7 and 337.9 mb/MeV for phonon (from 1 to 10 phonons) excitations at 75.5 MeV while experimental barrier distribution value is measured as 264.6 mb/MeV at 75.62 MeV in Fig. 1(b) [25]. At near the peak of the Coulomb barrier, our calculated barrier distribution results change as 427.2, 391.8, 390.4, 395.5 and 401.3 mb/MeV for phonon (from 1 to 10 phonons) excitations at 80.5 MeV while experimental barrier distribution value is measured as 431.8 mb/MeV at 80.61 MeV [25].

As can be seen from Figs. 1(a) and (b), the calculation model, codes, and parameters are in good agreement with experimental data [25]. Despite there are very small separations below the barrier region, all fusion cross-section calculations usually achieved a clear harmony with each other above the barrier region.

Barrier distributions soften when the phonon's number ascends. Barrier distributions alter mildly when phonons number is greater than , it attains its smooth at $n \approx 3$. In addition to this, the frame of barrier distributions sustains the same when a spacious number of phonons is considered in the coupled channel calculations.

The blue solid line, red solid line, purple ring, olive green solid line, and black plus line curves represent respectively the phonon excitations ($n=1, 2, 3, 5,$ and 10) of cross-sections were achieved over the interactions of the inert projectile and octupole (3^-) state of target nuclei in Fig. 2(a) [17-21]. Neon green stars and magenta circles represent CCFULL and Wong's Formula calculations [14,22-24]. Royal blue balls indicate experimental data for this reaction [25].

The three experimental data (for 73.19, 74.45, and 75.62 MeV) are slightly different from our theoretical calculations in Fig. 2(a). When we approached the barrier region, harmony was

observed between other theoretical and experimental values. Wong's formula cross-section calculations change as 22.26 mb at 78 MeV, 55.76 mb at 79 MeV, 102.50 mb at 80 MeV, 153.63 mb at 81 MeV, 205.02 mb at 82 MeV, 255.56 mb at 83 MeV, 304.98 mb at 84 MeV, 353.26 mb at 85 MeV, 400.42 mb at 86 MeV, 446.50 mb at 87 MeV, 491.53 mb at 88 MeV, 535.55 mb at 89 MeV, 578.59 mb at 90 MeV, 620.69 mb at 91 MeV, 661.87 mb at 92 MeV, 702.16 mb at 93 MeV, 741.60 mb at 94 MeV, 780.21 mb at 95 MeV and 818.01 mb at 96 MeV [23,24]. Experimental cross-section values are measured as 53.85 mb at 78.33 MeV, 95.85 mb at 80.61 MeV, 170.9 mb at 83.09 MeV, 298.4 mb at 86.32 MeV, 393 mb at 89.03 MeV and 553.7 mb at 95.05 MeV [25]. It is observed that coupled channel effects increased the fusion cross-section at energies around the Coulomb barrier.

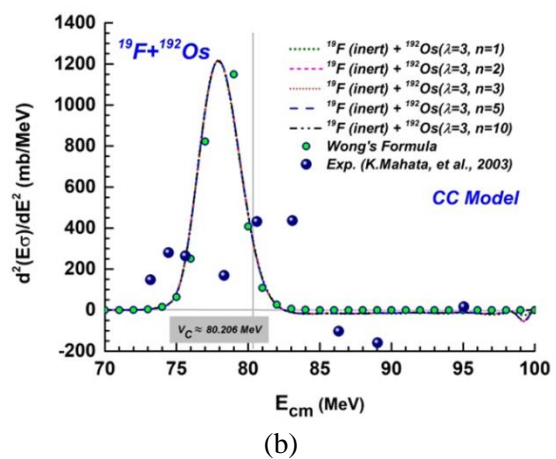
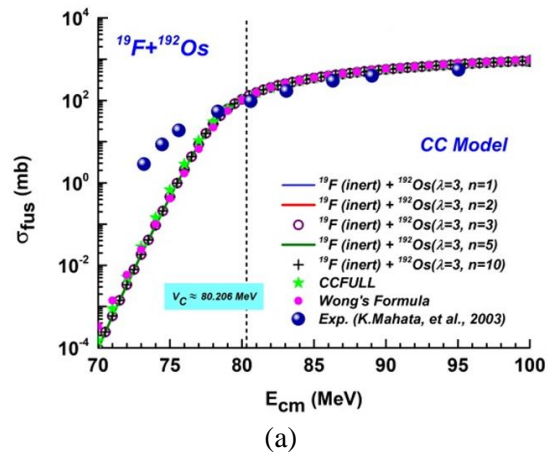


Fig. 2. Graphs of (a) the cross-sections and (b) barrier distributions for $^{19}F + ^{192}Os$ the fusion reaction within the coupled channel (CC) model the interactions of the inert projectile and octupole (3^-) state of target nuclei.

The olive green short dotted line, magenta short dashed line, red solid line, blue solid line, and

black dash-dot dotted line curves represent respectively the phonon excitations ($n=1, 2, 3, 5,$ and 10) of barrier distributions were achieved over the interactions of the inert projectile and octupole (3^-) state of target nuclei in Fig. 2(b) [17-21]. Royal blue circles filled with neon green represent Wong's Formula calculations [23,24]. Navy blue balls indicate experimental data for this reaction [25].

At near the peak of the Coulomb barrier, Wong's formula barrier distribution values change as 250.32 mb/MeV at 76 MeV and 407.42 mb/MeV at 80 MeV [23,24]. Experimental barrier distribution values are measured as 264.6 mb/MeV at 75.62 MeV and 431.8 mb/MeV at 80.61 MeV in Fig. 2(b) [25]. As can be seen from Figs. 2(a) and (b) calculations usually achieved a clear harmony with each other.

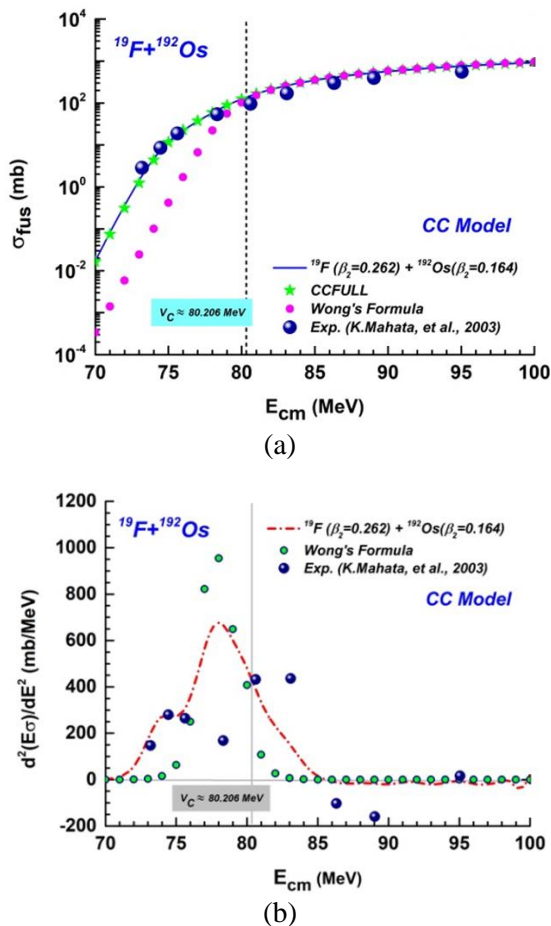


Fig. 3. Graphs of (a) the cross-sections and (b) barrier distributions for $^{19}F + ^{192}Os$ the fusion reaction within the coupled channel (CC) model the interactions of the deformed (rotational) projectile and target nuclei.

Furthermore, For $^{19}F + ^{192}Os$ reaction, in executing the coupled channels calculations, we also considered the deformed (rotational) projectile and target nuclei. The results were compared with

experimental data in Fig. 3. Figures 3(a,b) demonstrate fusion cross-sections and barrier distributions. We took the deformation parameter as $\beta_2 = 0.252$ and $\beta_4 = 0.180$ for projectile nucleus and $\beta_2 = 0.164$ and $\beta_4 = -0.077$ for target nucleus in this reaction [28-31]. Furthermore, we took the integration parameters as $R_{max} = 25fm$ and integration step $h = 0.05fm$ in our calculations [16,21,32].

The blue solid line curve represents cross-sections were achieved over the interactions of the deformed (rotational) projectile and target nuclei in Fig. 3(a) [17-21]. Also, neon green stars and magenta circles represent CCFULL and Wong's Formula calculations [14,22-24]. Royal blue balls indicate experimental data for this reaction [25].

All of the experimental data are in good agreement with our theoretical calculations in Fig. 3(a). When we approached the barrier region, harmony was observed between other theoretical and experimental values. NRV knowledge base cross-section calculations change as 2.694 mb at 73.5 MeV, 7.823 mb at 74.5 MeV, 16.56 mb at 75.5 MeV, 58.28 mb at 78 MeV, 144.4 mb at 80.5 MeV, 256.1 mb at 83 MeV, 417.6 mb at 86.5 MeV, 525.3 mb at 89 MeV and 756.4 mb at 95 MeV [17-21]. CCFULL cross-section calculations change as 1.24 mb at 73 MeV, 4.38 mb at 74 MeV, 22.66 mb at 76 MeV, 58.98 mb at 78 MeV, 124.73 mb at 80 MeV, 258.52 mb at 83 MeV, 400.22 mb at 86 MeV, 533.15 mb at 89 MeV and 764.23 mb at 95 MeV [14,22]. Experimental cross-section values are measured as 2.86 mb at 73.19 MeV, 8.57 mb at 74.45 MeV, 18.79 mb at 75.62 MeV, 53.85 mb at 78.33 MeV, 95.85 mb at 80.61 MeV, 170.9 mb at 83.09 MeV, 298.4 mb at 86.32 MeV, 393 mb at 89.03 MeV and 553.7 mb at 95.05 MeV [25]. It is observed that coupled channel effects increased the fusion cross section at energies around the Coulomb barrier.

The red short dash-dotted line curve represents respectively the barrier distributions were achieved over the interactions of the deformed (rotational) projectile and target nuclei in Fig. 3(b) [17-21]. Royal blue circles filled with neon green represents Wong's Formula calculations [23,24]. Navy blue balls indicate experimental data for this reaction [25].

At near the peak of the Coulomb barrier, NRV knowledge base barrier distribution values change as 174.2 mb/MeV at 73 MeV, 279.4 mb/MeV at 74.5 MeV, 287.7 mb/MeV at 75.5 MeV and 407.4 mb/MeV at 80.5 MeV [17-21]. Some of the

Wong's formula barrier distribution values change as 250.32 mb/MeV at 76 MeV and 407.42 mb/MeV at 80 MeV [23,24]. Experimental barrier distribution values are measured as 147.5 mb/MeV at 73.19 MeV, 280.2 mb/MeV at 74.45 MeV, 264.6 mb/MeV at 75.62 MeV and 431.8 mb/MeV at 80.61 MeV in Fig. 3(b) [25]. It is observed that the coupled channel effects reduce the barrier distribution values at energies above the Coulomb barrier in Fig. 3(b).

As can be seen from Figs. 3(a) and (b) our calculation model, codes and parameters are in good agreement with the experiment. Despite there are very small separations in the areas below the barrier region, all calculations usually achieved a clear harmony with each other above the barrier region for fusion cross-sections. NRV and Wong's formula calculations achieved a perfect harmony with each other and experimental data for barrier distributions [17-21,23,24].

Based on the information we have obtained from previous reaction calculations, we wanted to suggest and investigate a reaction in which experimental data are not available in the literature. For $^{18}\text{O} + ^{193}\text{Ir}$ reaction, in executing the coupled channels calculations, we considered the quadrupole (2^+) and octupole (3^-) states and phonon excitations of projectile nuclei while target nuclei were inert. Our calculation results are shown in Figs. 4 and 5. Figures 4(a,b) and 5(a,b) demonstrate fusion cross-sections and barrier distributions [33-35].

Results respectively represent phonons ($n=1, 2, 3, 5$ and 10) associated with quadrupole (2^+) and octupole (3^-) vibrations combinations of the surface of ^{18}O projectile nucleus via ($\lambda = 2^+, \hbar\omega_{2^+} = 1.9821 \text{ MeV}, \langle\beta_{2^+}^0\rangle = 0.347$) and ($\lambda = 3^-, \hbar\omega_{3^-} = 5.098 \text{ MeV}, \langle\beta_{3^-}^0\rangle = 0.595$) parameters [16-19]. Furthermore, we took the integration parameters as $R_{max} = 25 \text{ fm}$ and integration step $h = 0.05 \text{ fm}$ in our calculations [16,21,32].

The blue solid line, red solid line, purple ring, olive green solid line, and black plus line curves represent respectively the phonon excitations ($n=1, 2, 3, 5,$ and 10) of cross-sections were achieved over the interactions of quadrupole (2^+) state of the projectile and inert target nuclei in Fig. 4(a) [17-21]. Royal blue stars and soft magenta circles represent CCFULL and Wong's Formula calculations [14,22-24].

In Fig. 4(a), theoretical cross section calculations change as 0.0021, 0.00305, 0.00336, 0.00343, 0.00343 mb for phonon (from 1 to 10 phonons) excitations at 65 MeV and 182.6, 186.2,

186.8, 187, 187 mb for phonon (from 1 to 10 phonons) excitations at 75 MeV. CCFULL cross section calculations change as 0.00188 mb at 65 MeV and 172.49 mb at 75 MeV [14,22]. Wong's formula cross section calculations change as 0.00184 mb at 65 MeV and 172.46 mb at 75 MeV [23,24]. It is observed that coupled channel and phonon excitation effects increased the fusion cross sections at energies around the Coulomb barrier in Fig. 4(a).

The orange short dotted line, olive green short dashed line, magenta solid line, blue solid line, and black dash-dot dotted line curves represent respectively the phonon excitations ($n=1, 2, 3, 5,$ and 10) of barrier distributions were achieved over the interactions of quadrupole (2^+) state of the projectile and inert target nuclei in Fig. 4(b) [17-21]. Royal blue circles filled with neon green represent Wong's Formula calculations [23,24].

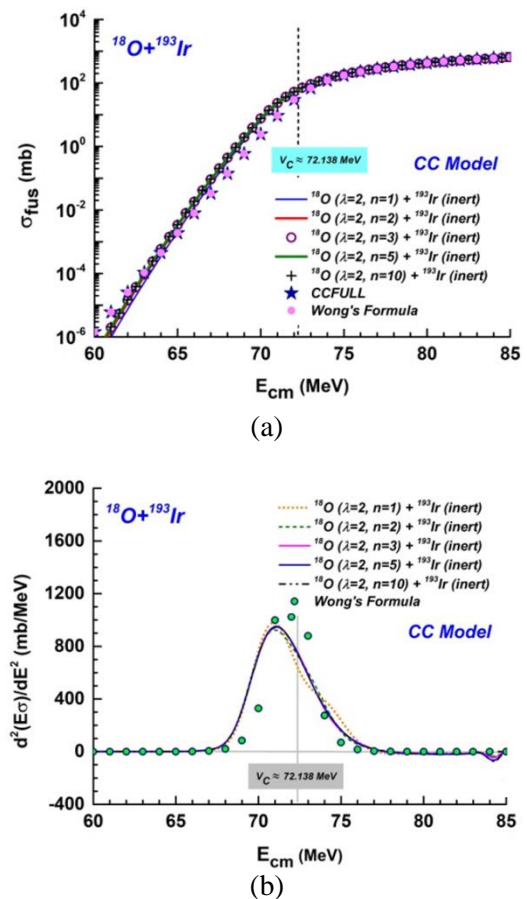


Fig. 4. Graphs of (a) the cross-sections and (b) barrier distributions for $^{18}\text{O} + ^{193}\text{Ir}$ the fusion reaction within the coupled channel (CC) model the interactions quadrupole (2^+) state of projectile nuclei and inert target nuclei.

Theoretical barrier distribution values change as 0.402, 0.563, 0.608, 0.617, 0.617 mb/MeV for phonon (from 1 to 10 phonons) excitations at 65 MeV, 999.9, 940, 957.6, 965.8, 965.1 mb/MeV

for phonon (from 1 to 10 phonons) excitations at 71 MeV and 2.177, 20.38, 18.64, 18.66, 17.74 mb/MeV for phonon (from 1 to 10 phonons) excitations at 77 MeV in Fig. 4(b). At near the peak of the Coulomb barrier, Wong's formula barrier distribution results change as 0.258 mb/MeV at 65 MeV, 997.84 mb/MeV at 71 MeV and 3.84286 mb/MeV at 77 MeV in Fig. 4(b) [23,24]. Barrier distributions softens when the phonons number ascends. Barrier distributions alters mildly when phonons number is greater than , it attains its smooth at $n \approx 3$. In addition to this, the frame of barrier distributions sustains same when a spacious number of phonons is considered in the coupled channel calculations.

As can be seen from Figs. 4(a) and (b) our calculation model, codes and parameters are in good agreement with each other. Despite there are very small separations in the areas below the barrier region, all calculations usually achieved a clear harmony with each other above the barrier region for fusion cross-sections.

The blue solid line, red solid line, purple ring, olive green solid line, and black plus line curves represent respectively the phonon excitations ($n=1, 2, 3, 5,$ and 10) of cross-sections was achieved over the interactions of octupole (3^-) state of the projectile and inert target nuclei in Fig. 5(a) [17-21]. Royal blue stars and soft magenta circles represent CCFULL and Wong's Formula calculations [14,22-24].

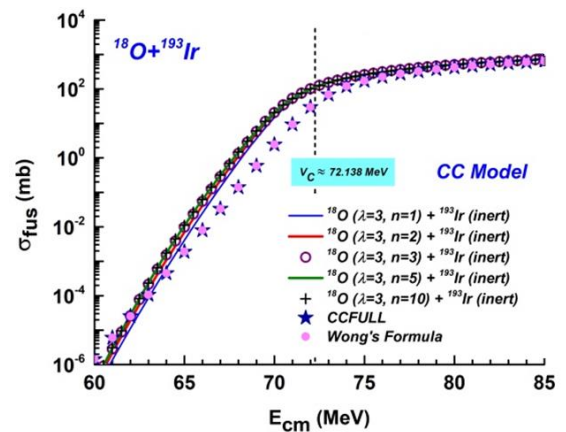
In Fig. 5(a), theoretical cross section calculations change as 0.00409, 0.00704, 0.00963, 0.01094, 0.011 mb for phonon (from 1 to 10 phonons) excitations at 65 MeV and 301.1, 309.6, 314.8, 313.2, 312.9 mb for phonon (from 1 to 10 phonons) excitations at 76 MeV. CCFULL cross section calculations change as 0.00185 mb at 65 MeV and 226.21 mb at 76 MeV [14,22]. Wong's formula cross section calculations change as 0.00182 mb at 65 MeV and 225.20 mb at 76 MeV [23,24]. It is observed that coupled channel and phonon excitation effects increased the fusion cross sections at energies around the Coulomb barrier in Fig. 5(a).

The orange short dotted line, olive green short dashed line, magenta solid line, blue solid line, and black dash-dot dotted line curves represent respectively the phonon excitations ($n=1, 2, 3, 5,$ and 10) of barrier distributions were achieved over the interactions of octupole (3^-) state of the projectile and inert target nuclei in Fig. 5(b) [17-21]. Royal blue circles filled with neon green represent Wong's Formula

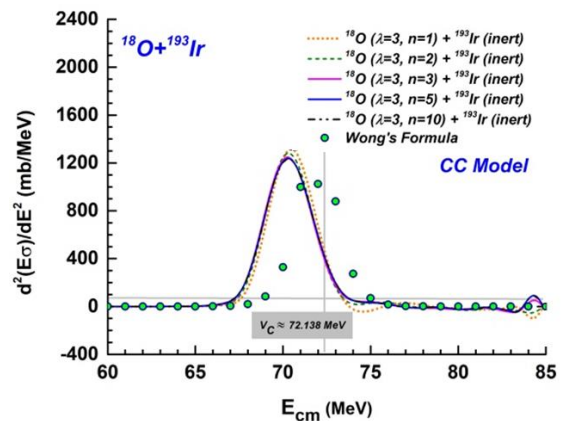
calculations [23,24].

Theoretical barrier distribution values change as 1239, 1147, 1102, 1106, 1106 mb/MeV for phonon (from 1 to 10 phonons) excitations at 71 MeV and 12.43, 33.47, 20.16, 18.59, 18.59 mb/MeV for phonon (from 1 to 10 phonons) excitations at 76 MeV in Fig. 5(b). At near the peak of the Coulomb barrier, Wong's formula barrier distribution results change as 997.84 mb/MeV at 71 MeV and 16.376 mb/MeV at 76 MeV [23,24] in Fig. 5(b). Barrier distributions soften when the phonon's number ascends. Barrier distributions alter mildly when phonons number is greater than , it attains its smooth at $n \approx 3$.

As can be seen from Figs. 5(a) and (b) all calculations usually achieved a good harmony with each other.



(a)



(b)

Fig. 5. Graphs of (a) the cross-sections and (b) barrier distributions for $^{18}\text{O} + ^{193}\text{Ir}$ the fusion reaction within the coupled channel (CC) model the interactions octupole (3^-) state of projectile nuclei and inert target nuclei.

Furthermore, for $^{18}\text{O} + ^{193}\text{Ir}$ reaction, in executing the coupled channels calculations,

we also considered the deformed (rotational) projectile and target nuclei. Figures 6(a,b) demonstrate fusion cross-sections and barrier distributions.

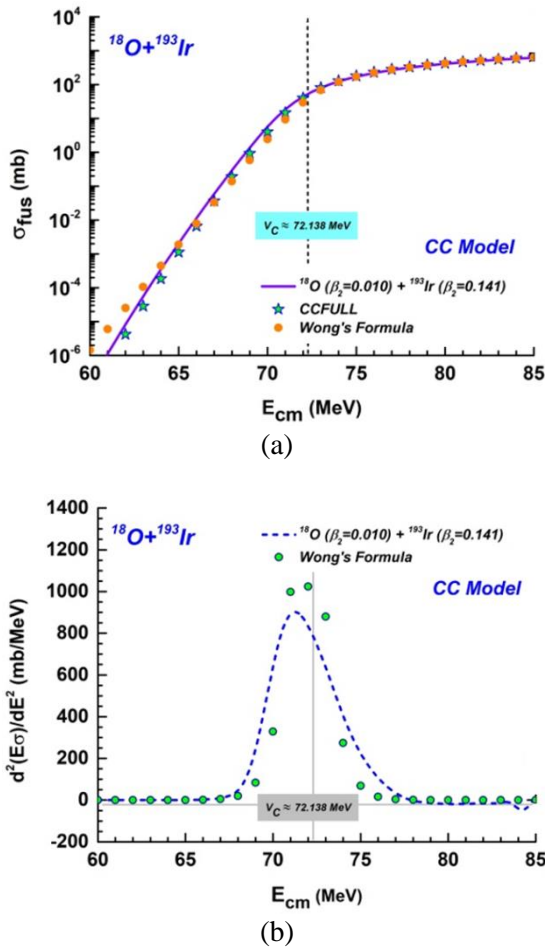


Fig. 6. Graphs of (a) the cross-sections and (b) barrier distributions for $^{18}\text{O} + ^{193}\text{Ir}$ the fusion reaction within the coupled channel (CC) model the interactions of the deformed (rotational) projectile and target nuclei.

We took the deformation parameter as $\beta_2 = 0.010$ and $\beta_4 = 0.141$ for projectile nucleus and $\beta_2 = 0.141$ and $\beta_4 = -0.066$ for target nucleus in this reaction [28-31]. Furthermore, we took the integration parameters as $R_{max} = 25\text{fm}$ and integration step $h = 0.05\text{fm}$ in our calculations [16,21,32].

The violet solid line curve represents cross-sections were achieved over the interactions of the deformed (rotational) projectile and target nuclei in Fig. 6(a) [17-21]. Also, neon green stars and orange circles represent CCFULL and Wong's Formula calculations [14,22-24].

In Fig. 6(a), NRV knowledge base cross section calculations change as 0.01139 mb at 66 MeV, 0.295 mb at 68 MeV, 5.66 mb at 70 MeV,

44.23 mb at 72 MeV, 123.7 mb at 74 MeV and 220.8 mb at 76 MeV [17-21]. CCFULL cross section calculations change as 0.007 mb at 66 MeV, 0.192 mb at 68 MeV, 4.038 mb at 70 MeV, 40.375 mb at 72 MeV, 129.23 mb at 74 MeV and 232.19 mb at 76 MeV [14,22]. Wong's formula cross section calculations change as 0.008 mb at 66 MeV, 0.140 mb at 68 MeV, 2.425 mb at 70 MeV, 29.932 mb at 72 MeV, 119.46 mb at 74 MeV and 225.20 mb at 76 MeV [23,24]. It is observed that coupled channel effects increased the fusion cross section at energies around the Coulomb barrier.

The blue short dashed line curve represents respectively the barrier distributions were achieved over the interactions of the deformed (rotational) projectile and target nuclei in Fig. 6(b) [17-21]. Royal blue circles filled with neon green represents Wong's Formula calculations [23,24].

At near the peak of the Coulomb barrier, NRV knowledge base barrier distribution values change as 0.381 mb/MeV at 65 MeV, 39.94 mb/MeV at 68 MeV, 907.5 mb/MeV at 71 MeV, 402.2 mb/MeV at 74 MeV and -3.812 mb/MeV at 78 MeV [17-21]. Some of the Wong's formula barrier distribution values change as 0.258 mb/MeV at 65 MeV, 20.048 mb/MeV at 68 MeV, 997.839 mb/MeV at 71 MeV, 273.77 mb/MeV at 74 MeV and 0.899 mb/MeV at 78 MeV [23,24]. It is observed that the coupled channel effects reduce the barrier distribution values at energies above the Coulomb barrier in Fig. 6(b).

As can be seen from Figs. 6(a) and (b) our calculation model, codes and parameters are in good agreement with each other. Despite there are very small separations in the areas below the barrier region, all calculations usually achieved a clear harmony with each other above the barrier region for fusion cross-sections. NRV and Wong's formula calculations achieved a perfect harmony with each other for barrier distributions [17-21,23,24].

CONCLUSION

This research was focused on the theoretical analysis through heavy-ion fusion on the examples of inspecting reactions of ^{211}At radionuclide by the interaction of stable nuclei. Especially, we have investigated the fusion cross-sections and the barrier distributions. The calculations were executed with the use of the web knowledge base NRV, CCFULL code, and Wong's Formula. Coupled channel (CC) model was employed for calculations. Coupled channel (CC) model is more ideal and convenient than other calculation methods for heavy-ion fusion

reactions. It can be seen in our theoretical calculation graphs that the fusion cross-section is compatible with each other in almost all nuclear parameter combinations at energies above the barrier while small differences or deviations are experienced for cross-sections calculations of energies at the sub-barrier. It is observed that coupled channel and phonon excitation effects increased the computed fusion cross-section at energies around the Coulomb barrier. Our results prove that the cross-sections will change and increase with the alter of energy and phonons. NRV Knowledge Base, CCFULL, and Wong's formula are useful, easy-to-understand, constantly updated, and innovative codes to gain and consolidate dexterities and experimentation in adapting to contemporary approximations to define the characteristics of nuclear nuclei and to be able to examine the parameters of nuclear interactions. The result that the attitude of the cross-sections in these energy intervals is entirely designated by the potential parameters has been accepted also by all researchers with many different types of research. More complex-different potentials and models can be used to further improve fusion calculations. In this manner, researches can be enriched by using new potentials and developing different algorithms for deformation parameters. Thus, by creating parameters that are best fitted with experimental research, we can obtain more reliable data to use these sets as simulations in the absence of experiments.

ACKNOWLEDGMENT

The authors declare that this paper is unfunded.

AUTHOR CONTRIBUTION

Z.M. Cinan performed all calculations, graphs and wrote the manuscript. T. Baskan and B. Erol critically overviewed the manuscript. A.H. Yilmaz supervised the research and critically overviewed the manuscript.

All authors read and approved the final version of the paper.

REFERENCES

1. A. M. Stefanini, G. Montagnoli, M. D'Andrea *et al.*, J. Phys. G: Nucl. Part. Phys. **48** (2021) 055101.

2. M. Singh, Sukhvinder and R. Kharab, Nucl. Phys. A **897** (2013) 179.
3. Vijay, R. P. Chahal, M. S. Gautam *et al.*, Phys. Rev. C **103** (2021) 024607.
4. H. C. Manjunatha, L. Seenappa, N. Sowmya *et al.*, Can. J. Phys. **99** (2021) 16.
5. N. K. Deb, K. Kalita, H. Al Rashid *et al.*, Phys. Rev. C **102** (2020) 034603.
6. M. Rashdan and T. A. Abdel-Karim, Int. J. Mod. Phys. E **29** (2020) 2050046.
7. M. Aversa, D. Abriola, M. A. G. Alvarez *et al.*, Phys. Rev. C **101** (2020) 044601.
8. M. V. Chushnyakova, M. Bhuyan, I. I. Gontchar *et al.*, Nuc. Phys. A **994** (2020) 121657.
9. P. W. Wen, O. Chuluunbaatar, A. A. Gusev *et al.*, Phys. Rev. C **101** (2020) 014618.
10. G. S. Li, J. G. Wang, J. Lubian *et al.*, Phys. Rev. C **100** (2019) 054601.
11. B. Sharifi and D. Naderi, Nuc. Phys. A **991** (2019) 121616.
12. R. Fereidonnejad, H. Sadeghi and M. Ghambari, Astrophys. Space Sci. **363** (2018) 50.
13. R. Gharaei and H. Hasanzade, Nuc. Phys. A **1013** (2021) 122223.
14. K. Hagino and N. Takigawa, Prog. Theor. Phys. **128** (2012) 1061.
15. M. Beckerman, Rep. Prog. Phys. **51** (1988) 1047.
16. V. I. Zagrebaev, *Heavy Ion Reactions at Low Energies*, in: Lecture Notes in Physics 963, 1st ed., Springer International Publishing, Berlin Heidelberg, Germany (2019) 156.
17. V. Karpov, A. S. Denikin, A. P. Alekseev *et al.*, Phys. At. Nucl. **79** (2016) 749.
18. Russian Foundation for Basic Research, NRV Web Knowledge Base on Low-Energy Nuclear Physics. <http://nrw.jinr.ru/>. Retrieved in January (2021).
19. M. A. Naumenko, V. V. Samarin, Yu. E. Penionzhkevich *et al.*, Bull. Russ. Acad. Sci. Phys. **80** (2016) 264.
20. A. V. Karpov, A. S. Denikin, A. P. Alekseev *et al.*, *NRV Web Knowledge Base on Low-Energy Nuclear Physics*, Proc. of All-Russia Conf. Sci. Serv. on the Internet (2015) 119.

21. A. S. Denikin, A. V. Karpov, M. A. Naumenko *et al.*, ALKU J. Sci. Special Issue (NSP 2018) (2019) 71.
22. M. Zamrun and K. Hagino, *Atom Indonesia* **36** (2010) 23.
23. C. Y. Wong, *Phys. Rev. Lett.* **31** (1973) 766.
24. N. W. Lwin, N. N. Htike and K. Hagino, *Phys. Rev. C* **95** (2017) 064601.
25. K. Mahata, S. Kailas, A. Shrivastava *et al.*, *Nuc. Phys. A* **720** (2003) 209.
26. D. L. Hill and J. A. Wheeler, *Phys. Rev.* **89** (1953) 1102.
27. N. Rowley, G. R. Satchler and P. H. Stelson, *Phys. Lett. B* **254** (1991) 25.
28. T. Kibedi and R. H. Spear, *At. Data Nucl. Data Tables* **80** (2002) 35.
29. P. Möller, A. J. Sierk, T. Ichikawa *et al.*, *At. Data Nucl. Data Tables* **109** (2016) 1.
30. B. Pritychenko, M. Birch, B. Singh *et al.*, *At. Data Nucl. Data Tables* **107** (2016) 1.
31. P. Raghavan, *At. Data Nucl. Data Tables* **42** (1989) 189.
32. B. Wang, K. Wen, W. J. Zhao *et al.*, *At. Data Nucl. Data Tables* **114** (2017) 281.
33. A. J. Najim, F. A. Majeed and K. H. H. Al-Attayah, *J. Eng. Appl. Sci.* **14** (2019) 10406.
34. A. Kaur and M. K. Sharma, *Indian J. Pure Appl. Phys.* **57** (2019) 576.
35. R. Wolski, *Phys. Rev. C* **93** (2016) 019802.